Mechanisms of Propagation of Intercellular Calcium Waves in Arterial Smooth Muscle Cells

Michèle Koenigsberger,[†] Dominique Seppey,[†] Jean-Louis Bény,[‡] and Jean-Jacques Meister[†*]
[†]École Polytechnique Fédérale de Lausanne (EPFL), Laboratory of Cell Biophysics, Lausanne, Switzerland; and [‡]Department of Zoology and Animal Biology, University of Geneva, Geneva, Switzerland

ABSTRACT In rat mesenteric arteries, smooth muscle cells exhibit intercellular calcium waves in response to local phenylephrine stimulation. These waves have a velocity of ~20 cells/s and a range of ~80 cells. We analyze these waves in a theoretical model of a population of coupled smooth muscle cells, based on the hypothesis that the wave results from cell membrane depolarization propagation. We study the underlying mechanisms and highlight the importance of voltage-operated channels, calcium-induced calcium release, and chloride channels. Our model is in agreement with experimental observations, and we demonstrate that calcium waves presenting a velocity of ~20 cells/s can be mediated by electrical coupling. The wave velocity is limited by the time needed for calcium influx through voltage-operated calcium channels and the subsequent calcium-induced calcium release, and not by the speed of the depolarization spreading. The waves are partially regenerated, but have a spatial limit in propagation. Moreover, the model predicts that a refractory period of calcium signaling may significantly affect the wave appearance.

INTRODUCTION

The regulation of hemodynamics by variations of the arterial diameter results from the contraction of smooth muscle cells (SMCs) present in the muscular arterial wall. Arterial contraction is caused by an increase in the smooth muscle cytosolic calcium concentration (1). Calcium increases result from the presence of vasoconstrictors in the vascular system. In vitro, calcium increases in vascular cells can be induced by receptor-ligand agonists like phenylephrine. The latter bind to cell-surface receptors, which activate phospholipase C and induce the release of the second messenger inositol 1,4,5-trisphosphate (IP_3). IP_3 then activates the release of calcium from the sarcoplasmic reticulum (2).

SMC calcium dynamics are often coordinated along the vascular wall. Vasomotion, a cyclic variation of the arterial diameter, is induced by synchronous calcium oscillations of SMCs (3–7). This synchronization is achieved by means of gap junctions (5,7). Gap junctions have been shown to play an important role in the intercellular communication between SMCs by enabling electrical communication and diffusion of calcium ions and IP_3 between neighboring cells (8–10). A membrane-potential depolarization propagation through gap junctions that leads to a spread of contraction along the arterial wall has often been observed in arterioles (11–13).

In rat mesenteric arteries, intercellular calcium waves induced by a local phenylephrine stimulation have been obtained previously in our laboratory (Fig. 1) (14). These waves exist only in the presence of a small global background stimulation of phenylephrine, and they have a velocity of ~20 cells/s and a range of ~80 cells. Moreover they are not influenced by the presence or absence of the endothelium (D. Seppey, J.L. Bény, and J.-J. Meister, unpublished results). This velocity is significantly faster than the speed that is expected from the diffusion of calcium or IP_3 by theoretical modeling (15–17). From electrophysiological experiments, it appears that the passage of current occurs rapidly over long distances in intact arteries (11,18,19). However the propagation of an electrical signal is also much faster than 20 cells/s (20,21).

The aim of this article is to analyze whether and how it is possible to obtain a wave range and velocity similar to those observed experimentally by assuming that an electrical communication underlies the calcium wave. We use our previously developed model (22) of a population of coupled SMCs to study these calcium waves. This model is able to reproduce the calcium dynamics of SMCs at different agonist concentrations (22). As the calcium waves are observed experimentally in the absence of endothelium (14), we do not include endothelial cells in our model. We stimulate locally a few SMCs and analyze the propagation of the electrical and calcium signals to the neighboring cells. We study the effects of different model parameter changes on the calcium wave range and velocity to determine the mechanisms underlying the waves. Our results are compared to the experimental findings obtained in our laboratory (14). Moreover, we show the possible effects of multiple consecutive wave inductions on the appearance of the calcium propagations.

EXPERIMENTAL BACKGROUND TO THE MODEL

Fig. 1 (14) shows intercellular calcium waves obtained on rat mesenteric arterial strips denuded of the endothelium.

Submitted January 24, 2010, and accepted for publication April 12, 2010.

*Correspondence: jean-jacques.meister@epfl.ch

Editor: Ian Parker.

0006-3495/10/07/0333/11 $2.00

doi: 10.1016/j.bpj.2010.04.031

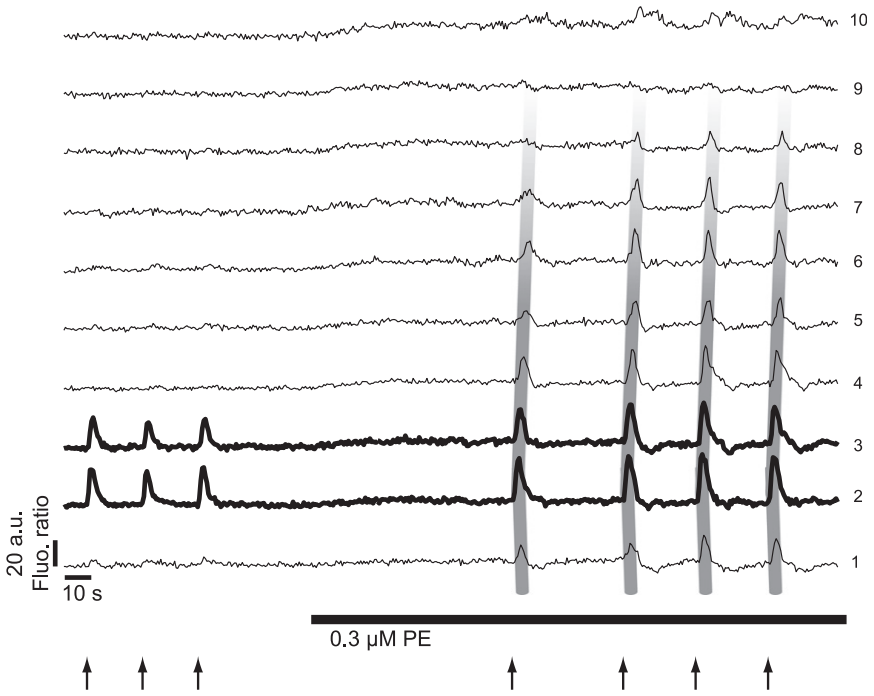

FIGURE 1 (Taken from Seppey et al. (14).) To analyze the intercellular calcium waves, 10 regions of interest of 30 × 75 μm^2, separated by a distance of 75 μm, were placed along the mesenteric arterial strip. The calcium concentration in the different regions of interest is proportional to the ratio of Fluo-4/Fura red fluorescence intensity. The figure shows typical time courses of the mean fluorescence ratio in the different regions of interest. The area that is locally stimulated is represented by bold curves, and broad gray lines have been added to better visualize the propagation of the mean fluorescence ratio increase along the arterial strip. Local stimulations of the strip with 40 μM phenylephrine (*arrows*) showed no fluorescence ratio increase, except in the stimulated area. There was no propagation when the artery was in its resting state. Combined with global stimulation with 0.3 μM phenylephrine (*PE*) (*horizontal bar*) through the superfusion system, the local stimulations induced a propagation of the mean fluorescence ratio increase that affected several regions of interest.

Experimental images encompass a strip of a length of ~700 μm. An area of a width of ~50 μm is locally stimulated with 40 μM phenylephrine. Local stimulations of the strip showed no calcium increase, except in the stimulated area. There was no propagation when the artery was in its resting state. Combined with a global stimulation of 0.3 μM phenylephrine through the superfusion system, the local stimulations induced propagation of an intercellular calcium wave. The range of this wave was 400 μm and its velocity 100 μm/s. Inhibitors of gap junctions and of voltage-operated calcium channels (VOCCs) abolished the waves.

MATHEMATICAL MODEL

The equations describing the calcium dynamics in SMCs are adapted from our previous article (22). This model takes into account the most relevant cellular mechanisms involved during the generation of calcium increases (23), and it is validated experimentally (22–26). The calcium dynamics in each SMC, i, is described by five variables: the calcium concentration in the cytosol, c_i; the calcium concentration in the sarcoplasmic reticulum, s_i; the cell membrane potential, v_i; the open-state probability, w_i, of calcium activated potassium channels; and the IP_3 concentration, I_i. Cells are connected to their nearest neighbors via gap-junctional electrical coupling.

The SMC model is given by

$$\frac{dc_i}{dt} = J_{IP3_i} - J_{SRuptake_i} + J_{CICR_i} - J_{extrusion_i} + J_{leak_i} - J_{VOCC_i} + J_{Na/Ca_i} \tag{1}$$

$$\frac{ds_i}{dt} = J_{SRuptake_i} - J_{CICR_i} - J_{leak_i}, \tag{2}$$

$$\frac{dv_i}{dt} = \gamma\left(- J_{Na/K_i} - J_{Cl_i} - 2J_{VOCC_i} - J_{Na/Ca_i} - J_{K_i} - J_{back_i}\right) + V_{coupling_i}, \tag{3}$$

$$\frac{dw_i}{dt} = \lambda(K_{activation_i} - w_i), \tag{4}$$

$$\frac{dI_i}{dt} = J_{PLC_{agonist_i}} - J_{degrad_i}. \tag{5}$$

The precise expressions of the various terms appearing in these two sets of nonlinear differential equations are given in the Appendix and are taken from Koenigsberger et al. (24). Crucial terms in the mathematical model include the gap-junctional electrical coupling (Eq. A12) and the VOCCs (Eq. A6), as the blockades of these channels have been studied experimentally (14). The term

$$J_{back_i} = G_{back}(v_i - v_{rest}) \tag{6}$$

has been added to model background currents. The term J_{Cli} is slightly changed to take into account that the channel is calcium-activated (27):

$$J_{Cl_i} = G_{Cl}\frac{c_i}{c_i + c_{Cl}}(v_i - v_{Cl}). \tag{7}$$

The addition of this calcium dependency is necessary to ensure a sufficient membrane depolarization after agonist stimulation and calcium increase.

TABLE 1 Parameter values for the SMC model

Parameter	Description	Value
F	Maximal rate of activation-dependent calcium influx	3.45 μM/s
K_r	Half-saturation constant for agonist-dependent calcium entry	1 μM
G_{Ca}	Whole-cell conductance for VOCCs	0.036195 μM mV^{-1} s^{-1}
v_{Ca_1}	Reversal potential for VOCCs	100.0 mV
v_{Ca_2}	Half-point of the VOCC activation sigmoidal	−24.0 mV
R_{Ca}	Maximum slope of the VOCC activation sigmoidal	8.5 mV
$G_{Na/Ca}$	Whole-cell conductance for Na^+/Ca^{2+} exchange	0.006 μM mV^{-1} s^{-1}
$c_{Na/Ca}$	Half-point for activation of Na^+/Ca^{2+} exchange by Ca^{2+}	0.5 μM
$v_{Na/Ca}$	Reversal potential for the Na^+/Ca^{2+} exchanger	−30.0 mV
B	SR uptake rate constant	49.5 μM/s
c_b	Half-point of the SR ATPase activation sigmoidal	1.0 μM
C	CICR rate constant	1545 μM/s
s_c	Half-point of the CICR Ca^{2+} efflux sigmoidal	2.0 μM
c_c	Half-point of the CICR activation sigmoidal	0.9 μM
D	Rate constant for Ca^{2+} extrusion by the ATPase pump	3.6 s^{-1}
v_d	Intercept of voltage dependence of extrusion ATPase	−100.0 mV
R_d	Slope of voltage dependence of extrusion ATPase	250.0 mV
L	Leak from SR rate constant	0.375 s^{-1}
γ	Scaling factor relating net movement of ion fluxes to the membrane potential (inversely related to cell capacitance)	492.5 mV/μM
$F_{Na/K}$	Net whole-cell flux via the Na^+-K^+-ATPase	0.03 μM/s
G_{Cl}	Whole-cell conductance for Cl^- current	0.6 μM mV^{-1} s^{-1}
c_{Cl}	Ca^{2+} sensitivity for Cl^- channels	0.7 μM
v_{Cl}	Reversal potential for Cl^- channels	−25.0 mV
G_K	Whole-cell conductance for K^+ efflux	0.045 μM mV^{-1} s^{-1}
v_K	Reversal potential for K^+	−94.0 mV
λ	Rate constant for net K_{Ca} channel opening	675.0
c_w	Translation factor for Ca^{2+} dependence of K_{Ca} channel activation sigmoidal	0 μM
β	Translation factor for membrane potential dependence of K_{Ca} channel activation sigmoidal	0.001 μM^2
v_{Ca_3}	Half-point for the K_{Ca} channel activation sigmoidal	−27.0 mV
R_K	Maximum slope of the K_{Ca} activation sigmoidal	12.0 mV
G_{back}	Whole-cell conductance for background currents	0.06 μM mV^{-1} s^{-1}
v_{rest}	Equilibrium potential	−55 mV
k	Rate constant of IP_3 degradation	0.1 s^{-1}
$J_{PLC_{agonist_b}}$	Rate of PLC activated by background agonist	0.05 μM/s
$J_{PLC_{agonist_s}}$	Rate of PLC activated by agonist in stimulated cells	0.4 μM/s
g	Electrical coupling coefficient	1000 s^{-1}

The meaning and values of all parameter values are given in Table 1. Several parameter values are changed with respect to our previous articles (22,24,25) so that our previous experimental results (14) can be reproduced. Changes in these parameter values are discussed in the Results and Discussion section.

Numerical methods

The model equations were solved using a fourth-order Runge-Kutta method. The equations were integrated on a two-dimensional grid of rectangular SMCs (Fig. 2 *a*) comprising 130 columns of cells. Assuming a typical size for a single SMC of 5 μm × 50 μm, our grid has a size of the same order as the experimental images (14). Within each SMC, the calcium and membrane potential dynamics are described by Eqs. 2–5. Each cell is connected with its nearest neighbors via electrical coupling.

To generate an intercellular wave, the 10 gray columns on the left in Fig. 2 *a* are stimulated for 1 s with a high agonist concentration (see Table 1). These cells are referred to henceforth as stimulated cells. The remaining cells (120 columns) experience a background agonist stimulation (see Table 1). In this way, we mimic our previous experimental setup (14). To describe the wave range and velocity we use the units cells and cells/s, respectively. By these units, we mean cells in the horizontal direction of Fig. 2 *a*, and these units are synonymous with columns and columns/s, respectively.

RESULTS AND DISCUSSION

Intercellular calcium wave and experimental comparison

Fig. 2 *b* shows an intercellular calcium wave obtained by exposing ten columns (Fig. 2 *a*, *stimulated cells*) to a high

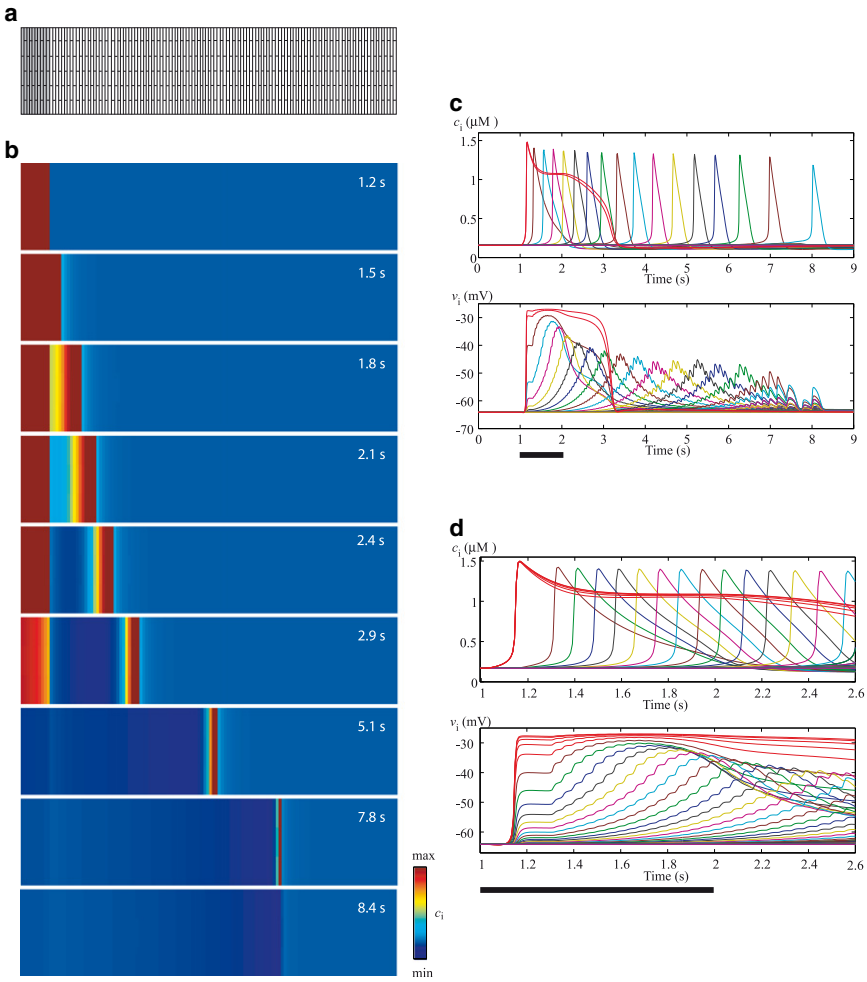

FIGURE 2 (*a*) The model equations are integrated on a two-dimensional grid of SMCs. As the typical size of a single SMC is 5 μm $\times$ 50 μm, the cell geometry is approximated by a rectangle. Each SMC is generally connected with its nearest neighbors via electrical coupling. To generate an intercellular wave, the 10 gray columns at the left are stimulated with a high agonist concentration for 1 s. The remaining cells (120 columns) experience a background agonist stimulation (see Table 1). (*b*) Intercellular calcium waves for the reference parameter set (Table 1). (*c*) Corresponding time courses of the calcium concentration, c_i (*upper panel*), and membrane potential, v_i (*lower panel*), in a cell of every fifth column. The red curves correspond to the stimulated cells. The bar indicates the period (1 s) during which the stimulated cells experience a high agonist concentration. (*d*) Zoom of the time interval 1–1.6 s: time courses of the calcium concentration, c_i (*upper panel*), and membrane potential, v_i (*lower panel*), in a cell of every second column.

agonist concentration $J_{\mathrm{PLC}_{\mathrm{agonist_s}}}$ (see Table 1) for 1 s. The remaining cells experience a background agonist stimulation (see Table 1). In this way, we reproduce our previous experimental setup (14). We observe that an intercellular calcium wave is propagating over a large part of the grid, with a limited range. Fig. 2 *c* gives the time evolution of the calcium concentration and membrane potential in individual SMCs. For clarity, Fig. 2 *d* shows a close-up of the first 2.6 s of Fig. 2 *c*. We observe that after an agonist stimulation lasting 1 s, the membrane potential and calcium concentration are transmitted beyond the stimulated cells for ~7 s.

After the agonist stimulation, the stimulated cells exhibit calcium elevation accompanied by membrane depolarization. This depolarization results from outward chloride currents through calcium-activated chloride channels (Eq. 7). It is instantaneously electrotonically transmitted to neighboring cells with a decay in amplitude over distance (Fig. 2 *d*), and opens VOCCs (Eq. A6) in these cells. After a small delay (see Fig. 2 *d*), a sufficient amount of calcium has entered the cell, and calcium-induced calcium release (CICR; Eq. A3) is activated, leading to a calcium flash. The time delay after which CICR is triggered is smallest in cells that are direct neighbors of the stimulated cells, as these cells are exposed to stronger membrane-potential depolarizations. The calcium increase further depolarizes the cells due to calcium-activated chloride channels, and this depolarization is further transmitted to other cells and added to the existing depolarization. The regenerated depolarization then enhances the calcium entry through VOCCs activating CICR. In this way, the calcium wave can be regenerated over long distances. Note that the membrane potential in each cell exhibits low-amplitude oscillations resulting from coupling with the membrane potentials of neighboring cells.

With the set of parameters given in Table 1, the model is able to reproduce the experimental observations (Fig. 1) (14). The wave range of 76 cells and the wave velocity of ~20 cells/s correspond to experimental measurements of a 400 μm wave range and 100 μm/s velocity, assuming an SMC width of 5 μm (Fig. 2 *a*). The calcium wave results from the spread of a depolarizing electrical signal, but it is slower than the electrical propagation, which is instantaneously electrotonically transmitted. The velocity of the calcium wave is limited by the time needed for calcium influx through VOCCs and by the subsequent CICR, not

by the speed of spreading of the depolarization (see Fig. 2 *d*). Note that the velocity decreases with distance (see Fig. 2 *c*). These results are also obtained using other theoretical models (15,16). However, they have not been observed experimentally (14), possibly due to lack of resolution. In the following text, the velocity shown in the figures is the instant velocity of the cells located close to the stimulated cells, and its value is similar for all cells in that vicinity.

A theoretical model describing regenerated intercellular calcium waves in glial cells has been elaborated by Höfer et al. (17). In this model, the waves propagate through IP_3 diffusion and are regenerated by phospholipase C-δ activity. As in our study, the regenerated wave propagation has a spatial limit. This unexpected partial regenerated behavior can be explained in our study. As the stimulated cells are exposed to a high agonist concentration, the membrane depolarization resulting from this agonist stimulation is higher than those regenerated in the other cells. Both types of membrane potential depolarizations propagate electrotonically to neighboring cells. However, the depolarization resulting from propagation of the regenerated membrane potential is lower than that induced by propagation of the membrane potential of the stimulated cells. Since the electrotonic membrane potential propagation leads to an exponential decay in membrane potential depolarization over distance, far from the stimulated cells the amount of calcium entering the cells through VOCCs is not sufficient to activate CICR and induce a calcium flash. Thus, partly regenerated waves only exist because the membrane potential depolarization in the stimulated cells is higher than that regenerated in the follower cells. We will see below that with different parameter values the waves can be completely regenerated.

The set of parameters in Table 1 was chosen to reproduce the experimental observations (range, velocity) in our laboratory (14). To unravel the mechanisms underlying these waves, we studied the effect of several system parameters on wave propagation.

Parameters influencing wave velocity and range

Fig. 3 gives the range and velocity of the wave as a function of different parameters: the electrical coupling coefficient, the VOCC conductance, the amplitude of CICR, the chloride channel conductance, the magnitude of the background agonist stimulation, and the number of stimulated cells. In experiments, it was not possible to gradually change channel conductance, and channels were either pharmacologically inhibited or not (14). Here we increase the parameter values incrementally to gain a better understanding of the intercellular waves. Changes in the parameter values are discussed below. Note that we keep the initial value of the VOCC conductance, CICR amplitude, and chloride channel conductance (Table 1) in the stimulated cells and vary only these parameter values in the other cells. This allows us to better analyze the effects of different parameter values on the wave characteristics without influencing the stimulated-cell signal.

Electrical coupling

The electrical coupling coefficient (Fig. 3 *a*) is responsible for the propagation of membrane depolarization. Decreasing this coefficient diminishes the wave range and velocity. Indeed, the amplitude of the electrotonic spreading of the wave is more rapidly reduced over distance. This decreases calcium entry through VOCCs, and the threshold for CICR is reached in fewer cells. Setting the electrical coupling coefficient to zero completely inhibits the wave, in agreement with experimental findings (Fig. 3 in our previous study (14)). Sufficiently high values of this coefficient lead to fully regenerated waves, i.e., waves that have no limit in the range of propagation and propagate over the whole grid (Fig. 2 *a*). Similar results have been obtained in another theoretical model (17), where high values of the gap-junctional permeability for IP_3 may also result in completely regenerated IP_3-mediated calcium waves.

The value of the electrical coupling coefficient used in Fig. 2 ($g = 1000\ s^{-1}$; Table 1) to reproduce the experimental findings is the same one used in our previous articles (22,24,25), and corresponds to the gap-junctional conductance measured experimentally (28–31).

VOCC conductance

Increasing the VOCC conductance (Eq. A6) (Fig. 3 *b*) enhances the entry of extracellular calcium for a given membrane potential value. The threshold for CICR is therefore reached more rapidly (increased wave velocity) and in more cells (increased wave range). A sufficiently high conductance leads to fully regenerated calcium waves. Setting this conductance to zero completely inhibits the calcium wave; only the electrotonic propagation of membrane potential to neighboring cells is preserved. This reproduces our experimental observations, described previously (14), that wave propagation is inhibited by the addition of nifedipine (see Fig. 5 in that study). In a similar way, Fig. 6 of that study showed that the addition of Bay K 8644, a VOCC activator, enhanced wave propagation (14).

CICR amplitude

Higher CICR amplitude (Eq. A3 and Fig. 3 *c*) results in a lower calcium concentration threshold for a calcium flash. Sufficiently high CICR amplitudes lead to fully regenerated calcium waves, whereas a zero amplitude abolishes the wave.

Chloride channel amplitude

In our model, the chloride channels (Eq. 7 and Fig. 3 *d*) are necessary for the membrane potential depolarization after a calcium increase, in this way regenerating the membrane potential. Setting their conductance to zero does not

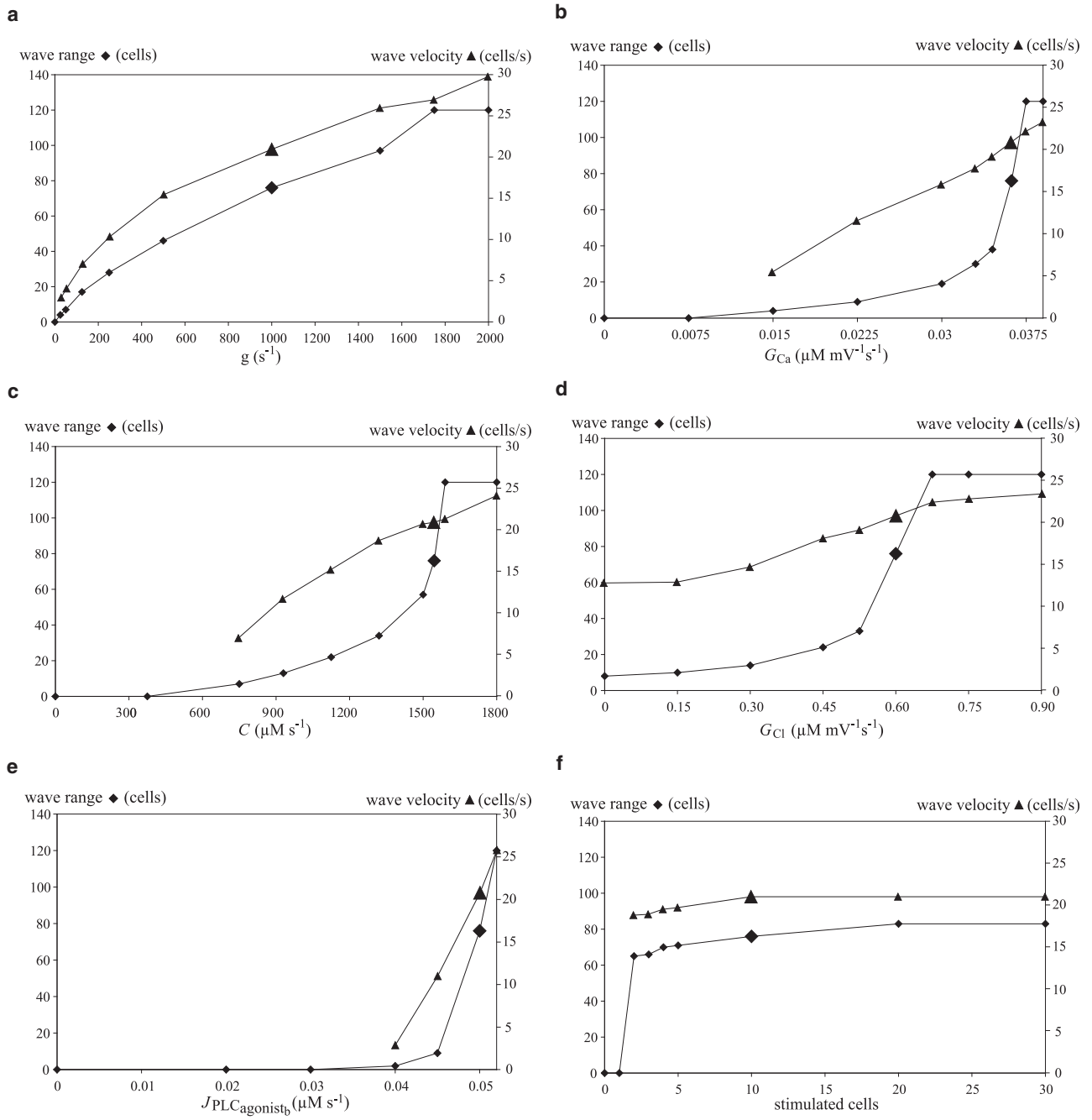

FIGURE 3 Range (*diamonds*) and velocity (*triangles*) of the calcium wave as a function of the electrical coupling coefficient g (*a*), the VOCC conductance, G_{Ca} (*b*), the amplitude of CICR C (*c*), the amplitude of the chloride channel, G_{Cl} (*d*), the magnitude of the background agonist stimulation, $J_{PLC_{agonist_b}}$ (*e*), and the number of columns of stimulated cells (*f*). The large diamond and triangle in each panel correspond to the reference parameter set (Table 1).

completely inhibit the calcium wave, as the membrane potential is still electrotonically transmitted, leading to calcium increase through VOCCs and CICR in the neighboring cells. However, after the calcium increase in these cells, the membrane potential is not further depolarized and regenerated, which limits the range of propagation of the calcium wave. Sufficiently high conductances may amplify the membrane depolarization in all cells, also leading to a fully regenerated wave.

The conductance value used in Fig. 2 (Table 1) to reproduce the experimental observations leads to an amplitude of membrane potential depolarization after phenylephrine stimulation that is in agreement with experimental data (32,33).

Background agonist stimulation

In the absence of any background agonist stimulation, $J_{PLC_{agonist_b}}$ (Fig. 3 *e*), there is no wave propagation, in

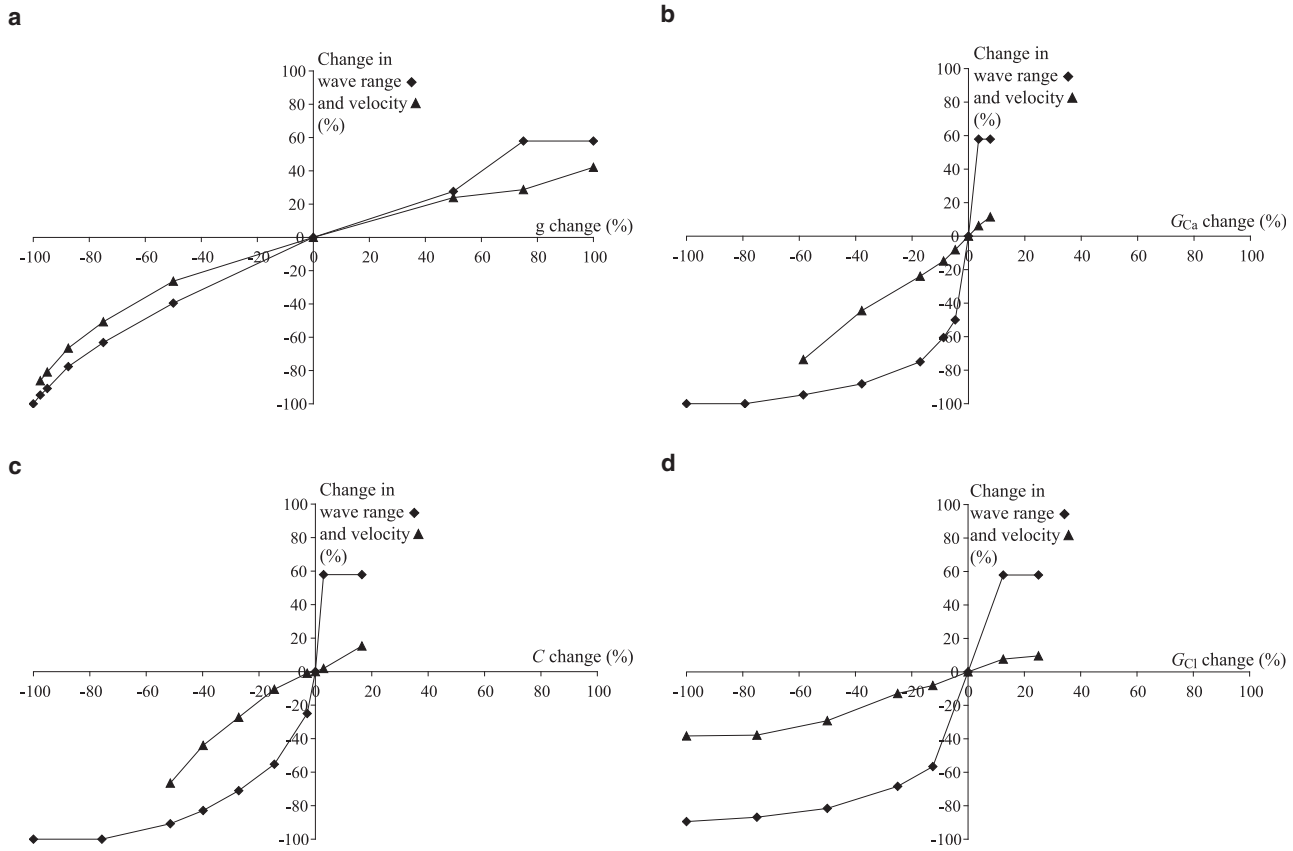

FIGURE 4 Relative wave range (*diamonds*) and velocity (*triangles*) changes as a function of relative parameter changes in the electrical coupling coefficient g (*a*), conductance of VOCCs, G_{Ca} (*b*), amplitude of CICR, C (*c*), and conductance chloride channels, G_{Cl} (*d*). The reference point (0%) corresponds to the parameter values in Table 1.

agreement with experimental observations (Fig. 1). Increasing the background stimulation increases the IP_3 concentration (Eq. 5) and, subsequently, the cytosolic calcium concentration (Eq. A1), approaching in this way the threshold for CICR necessary for a calcium flash. Note that the background agonist concentrations used do not give rise to any spontaneous calcium flashes.

Number of stimulated cells

The number of stimulated cells (first 10 columns in Fig. 2 *a*) (Fig. 3 *f*) was chosen to match the experimental setting (14). Decreasing the number of stimulated cells decreases the wave range. One stimulated column (cell) is not enough to induce a calcium wave using the reference parameter set (Table 1). An elevated membrane potential of a single column is not strong enough to entrain its neighboring cells. The transmission of the membrane potential to the neighboring cells reduces the depolarization in the stimulated column, and the transmitted membrane potential in the neighboring cells is not sufficient for significant calcium entry through VOCCs. Increasing the number of stimulated cells beyond 10 columns does not have any more of a significant effect on the wave velocity and range.

Thus, there are some essential mechanisms for intercellular wave propagation: gap-junctional electrical coupling is necessary for propagation of cell membrane depolarization, VOCCs for calcium entry after a depolarization, CICR for a calcium flash, and chloride channels for regeneration of depolarization after the calcium increase. The model is in agreement with our previously published experimental study (14). It confirms the involvement of gap junctions, VOCCs, and background agonist stimulation and predicts the importance of CICR, chloride channels, and the size of the agonist-stimulated area. Similar mechanisms have been found to be crucial for synchronization of nonidentical cells in a theoretical model based on experimental findings in fibroblasts (34). However, that model did not focus on the wave range and velocity.

In summary, both the wave velocity and range increase when the different parameter values increase. When fully regenerated waves are obtained, the wave range stays constant (equalling the number of nonstimulated cells in the grid in Fig. 2 *a*), whereas the wave velocity continues to increase. Fig. 4 shows the relative changes in velocity and range as a function of relative parameter changes in the electrical coupling coefficient, conductance of VOCCs,

amplitude of CICR, and chloride channel conductance. It thus provides a quantitative comparison of the effects of these parameters. The reference point (0%) corresponds to the parameter values in Fig. 2 and Table 1. By comparing the different elements of Fig. 4, we can see that wave range and velocity depend less strongly on the electrical coupling coefficient than on the other parameters for small parameter changes. Moreover, the wave velocity is less affected by parameter changes than the wave range.

Refractory period

In vivo, SMCs may be subject to multiple stimuli by agonists. If one stimulus occurs rapidly after another, the SMCs may be in a refractory period of calcium signaling in our model. The wave propagation may then be less efficient. Indeed, the intracellular stores are not yet replenished and CICR cannot be triggered. Fig. 5 shows a density plot of three intercellular calcium waves. The stimulated cells are exposed to three identical subsequent agonist stimulations lasting 1 s each. The first stimulus gives rise to a fully regenerated calcium wave propagating to all cells. The second stimulus, occurring about 4 s after the first, is strong enough to induce a calcium increase and a depolarization in the stimulated cells, but the range of the subsequent intercellular calcium wave is only a few cells. This is due to the fact that the cells are in a refractory period during which the internal stores are not yet replenished. Even if the depolarization propagates to all cells and calcium enters through VOCCs, CICR is not triggered and the cells are not able to respond with a calcium increase. After the third stimulus, which occurs 2 s after the second, the cells that responded after the second stimulus are still in a refractory period and do not exhibit a calcium rise. However, the cells that are not direct neighbors of the stimulated cells, and which did not respond after the second stimulus, are not in the refractory period anymore. They can thus exhibit calcium increases resulting from the electrotonic propagation of the depolarization. There is a seeming pacemaker region, as a wave is starting from these unstimulated cells. Thus, when cells are submitted to multiple stimuli, there may be waves departing from nonstimulated regions due to the existence of a refractory period. This model prediction suggests that regions from which calcium and contraction waves are observed to arise may not necessarily be stimulated regions.

Discussion of model hypotheses

We analyze only the effects of electrical communication, without taking into account intercellular calcium or IP_3 diffusion. This allows us to better analyze and understand the mechanisms underlying calcium waves resulting from electrical coupling. Intercellular calcium waves induced by local agonist or mechanical stimulation and resulting from calcium and IP_3 diffusion have been studied extensively

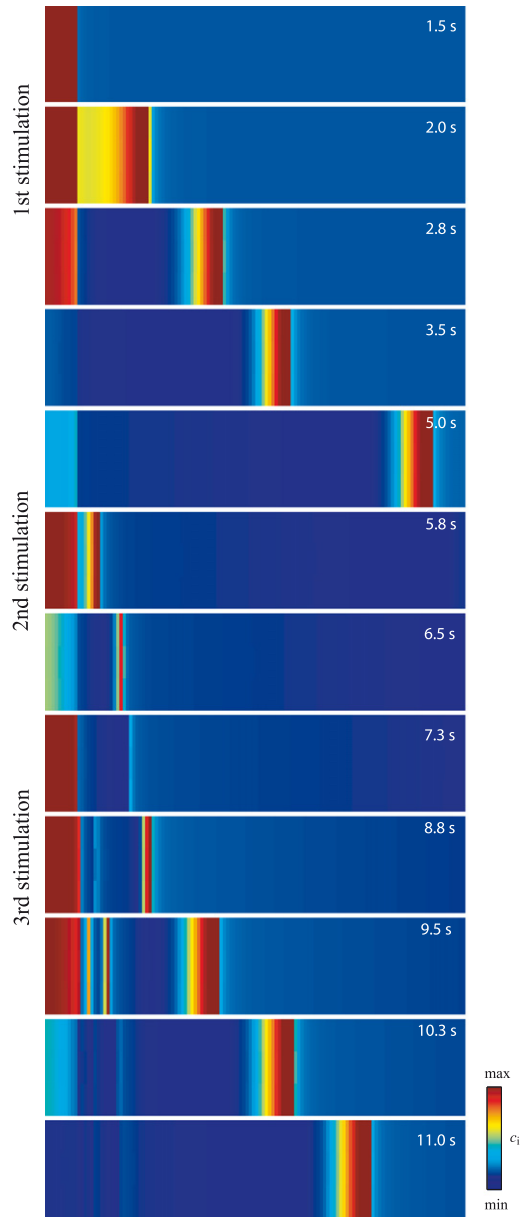

FIGURE 5 Density plot of intercellular calcium waves ($G_{Ca} = 0.039\ \mu M\ mV^{-1}\ s^{-1}$). The stimulated cells are exposed to three subsequent agonist stimulations of 1-s duration occurring at times $t = 1$ s, $t = 4.75$ s, and $t = 6.75$ s.

from a theoretical point of view (15–17), and the wave speed obtained using these models cannot account for that measured experimentally. Note, however, that calcium coupling may be sufficient to synchronize oscillating cells (22,35) that are globally stimulated by agonists. There is probably an overlap between IP_3, calcium, and membrane potential propagation at the start of the wave, and IP_3 or calcium diffusion may slightly increase the wave velocity at the start of the wave.

To simplify our study, we did not include endothelial cells in our model, as calcium waves produced experimentally

have been obtained in the absence of endothelium (14). We have studied the detailed effects of the endothelium on SMC calcium dynamics and vasomotion in a previous article (24).

The equation modeling chloride channels has been modified with respect to our previous articles (22,24–26) to take into account that it is calcium-activated. In this way, we were able to reproduce the depolarization accompanying a calcium increase and to counteract the hyperpolarizing effect of calcium-activated potassium channels. The depolarization induced by the Na^+/Ca^{2+} exchanger (Eq. A7) is not strong enough to sufficiently regenerate the waves. Indeed, a high amplitude of this exchanger depolarizes the cell after a calcium increase, but it also removes calcium from the cell, which in turn is hyperpolarizing. The cell membrane also depolarizes after calcium entry through VOCCs, as calcium is a positive ion. However, this depolarization is not significant in our model, and VOCCs are also not able to induce a depolarization after a calcium flash resulting from CICR. In our model, CICR occurs through ryanodine receptors, as calcium flashes and oscillations are inhibited by blockade of these receptors in rat mesenteric arteries (4). CICR may also occur through the IP_3 receptors, as IP_3 receptors can be activated and inactivated by a calcium increase (36). However, the experimentally determined peak calcium concentration values for activation of the IP_3 receptor differ significantly among experimental setups, and it is uncertain whether CICR can occur for the range of calcium and low IP_3 concentrations obtained in our model (37). Including a calcium sensitivity of the IP_3 receptor would modulate our results by increasing or decreasing the wave velocity and range, depending on the particular model parameters chosen.

The main findings of our study are that intercellular calcium waves with the same range and velocity as seen experimentally can be generated through electrical propagation, and that the time needed for calcium flash generation, not the speed of electrical propagation, is the limiting factor in wave velocity. These conclusions are not dependent on model details or on the particular choice of model, as long as the model presents a term generating a depolarization after agonist stimulation, a term modeling calcium influx after a depolarization, and a term responsible for a calcium flash.

The size of the grid of the population of SMCs (Fig. 2 *a*) has been chosen to correspond to the experimental images obtained in our laboratory (14). When the wave approaches the end of the grid, it may be exposed to some border effects, as the propagation of the membrane potential is stopped at the borders. Membrane potential is therefore more depolarized in the border cells than it would have been if no border were present, because it is not damped by neighboring cells with lower membrane potential. Wave propagation is then facilitated. Completely regenerated waves would be obtained for lower values of electrical coupling, VOCC conductance, and CICR amplitude if the grid were smaller.

In our laboratory, intercellular calcium waves arising under global homogeneous agonist stimulation have also been observed (14). On one arterial segment, the waves are always observed to depart from the same region. The nature of these pacemaker regions is so far undetermined. Further investigation of this issue could give rise to another modeling study.

CONCLUSIONS

Our model is a rigorous test of the hypothesis that intercellular calcium waves observed in arterial SMCs that exhibit a velocity of ~20 cells/s may result from electrical coupling. The velocity of the calcium wave is much smaller than the speed of propagation of an electrical signal. It is limited by the time needed for generation of a calcium flash, not by the speed of spreading of the depolarization. The waves are regenerated, but they have a spatial limit in propagation. These results are not dependent on our particular choice of model. In our model, VOCCs are necessary for calcium entry after a depolarization, CICR is essential for the calcium flash, and chloride channels induce regeneration of depolarization after a calcium increase. Thus, our model has allowed us to reproduce, and gain a better understanding of, our previously published experimental findings (14). Moreover, the model predicts that a refractory period of calcium signaling may have significant effects on the appearance of the wave: the starting point of the wave may not necessarily be a stimulated region, but a region of cells that are not in a refractory period.

APPENDIX A: DETAILS OF THE MATHEMATICAL MODEL

The various terms appearing in Eqs. 2–5 are described by the following expressions, as presented previously (22–26). The calcium flux,

$$J_{IP3_i} = F\frac{I_i^2}{K_r^2 + I_i^2}, \tag{A1}$$

models the calcium release from IP_3-sensitive stores,

$$J_{SRuptake_i} = B\frac{c_i^2}{c_i^2 + c_b^2} \tag{A2}$$

models the SR/ER uptake,

$$J_{CICR_i} = C\frac{s_i^2}{s_c^2 + s_i^2}\frac{c_i^4}{c_c^4 + c_i^4} \tag{A3}$$

describes the CICR,

$$J_{extrusion_i} = Dc_i\left(1 + \frac{v_i - v_d}{R_d}\right) \tag{A4}$$

is the calcium extrusion by Ca^{2+}-ATPase pumps,

$$J_{leak_i} = Ls_i \tag{A5}$$

corresponds to the leak from the SR,

$$J_{\mathrm{VOCC_i}} = G_{\mathrm{Ca}}\frac{v_\mathrm{i} - v_{\mathrm{Ca_1}}}{1 + e^{-[(v_\mathrm{i}-v_{\mathrm{Ca_2}})/R_{\mathrm{Ca}}]}} \tag{A6}$$

is the calcium influx through VOCCs, and

$$J_{\mathrm{Na/Ca_i}} = G_{\mathrm{Na/Ca}}\frac{c_\mathrm{i}}{c_\mathrm{i} + c_{\mathrm{Na/Ca}}}\left(v_\mathrm{i} - v_{\mathrm{Na/Ca}}\right) \tag{A7}$$

is the Na^+/Ca^{2+} exchange.

$$J_{\mathrm{Na/K_i}} = F_{\mathrm{Na/K}} \tag{A8}$$

is the Na^+-K^+-ATPase,

$$J_{\mathrm{Cl_i}} = G_{\mathrm{Cl}}\frac{c_\mathrm{i}}{c_\mathrm{i} + c_{\mathrm{Cl}}}(v_\mathrm{i} - v_{\mathrm{Cl}}) \tag{A9}$$

models the chloride channels,

$$J_{\mathrm{K_i}} = G_{\mathrm{K}} w_\mathrm{i}(v_\mathrm{i} - v_{\mathrm{K}}) \tag{A10}$$

is the K^+ efflux,

$$J_{\mathrm{back_i}} = G_{\mathrm{back}}(v_\mathrm{i} - v_{\mathrm{rest}}) \tag{A11}$$

corresponds to background currents,

$$V_{\mathrm{coupling_i}} = -g\sum_{\mathrm{k}}(v_\mathrm{i} - v_\mathrm{k}) \tag{A12}$$

models the electrical coupling,

$$K_{\mathrm{activation_i}} = \frac{\left(c_\mathrm{i} + c_\mathrm{w}\right)^2}{\left(c_\mathrm{i} + c_\mathrm{w}\right)^2 + \beta e^{-[(v_1 - v_{\mathrm{Ca_3}})/R_{\mathrm{K}}]}} \tag{A13}$$

describes the calcium and voltage activation of K^+ channels, and the IP_3 flux,

$$J_{\mathrm{degrad_i}} = kI_\mathrm{i}, \tag{A14}$$

models the IP_3 degradation. The constant $J_{\mathrm{PLC_{agonist_b}}}$ is the rate of PLC activated by agonists. The parameter values for the SMC model are given in Table 1.

This research was supported by Swiss National Science Foundation grants FN 31000-114097 and 310030-127122.

REFERENCES

1. Meininger, G. A., D. C. Zawieja, …, J. P. Davey. 1991. Calcium measurement in isolated arterioles during myogenic and agonist stimulation. *Am. J. Physiol.* 261:H950–H959.
2. Minneman, K. P. 1988. α1-adrenergic receptor subtypes, inositol phosphates, and sources of cell Ca^{2+}. *Pharmacol. Rev.* 40:87–119.
3. Mauban, J. R., C. Lamont, …, W. G. Wier. 2001. Adrenergic stimulation of rat resistance arteries affects Ca^{2+} sparks, Ca^{2+} waves, and Ca^{2+} oscillations. *Am. J. Physiol. Heart Circ. Physiol.* 280:H2399–H2405.
4. Peng, H., V. Matchkov, …, H. Nilsson. 2001. Hypothesis for the initiation of vasomotion. *Circ. Res.* 88:810–815.
5. Sell, M., W. Boldt, and F. Markwardt. 2002. Desynchronising effect of the endothelium on intracellular Ca^{2+} concentration dynamics in vascular smooth muscle cells of rat mesenteric arteries. *Cell Calcium.* 32:105–120.
6. Lamboley, M., A. Schuster, …, J. J. Meister. 2003. Recruitment of smooth muscle cells and arterial vasomotion. *Am. J. Physiol. Heart Circ. Physiol.* 285:H562–H569.
7. Haddock, R. E., and C. E. Hill. 2005. Rhythmicity in arterial smooth muscle. *J. Physiol.* 566:645–656.
8. Christ, G. J., A. P. Moreno, …, D. C. Spray. 1992. Gap junction-mediated intercellular diffusion of Ca^{2+} in cultured human corporal smooth muscle cells. *Am. J. Physiol.* 263:C373–C383.
9. Little, T. L., J. Xia, and B. R. Duling. 1995. Dye tracers define differential endothelial and smooth muscle coupling patterns within the arteriolar wall. *Circ. Res.* 76:498–504.
10. Christ, G. J., D. C. Spray, …, P. R. Brink. 1996. Gap junctions in vascular tissues. Evaluating the role of intercellular communication in the modulation of vasomotor tone. *Circ. Res.* 79:631–646.
11. Xia, J., and B. R. Duling. 1995. Electromechanical coupling and the conducted vasomotor response. *Am. J. Physiol.* 269:H2022–H2030.
12. Welsh, D. G., and S. S. Segal. 1998. Endothelial and smooth muscle cell conduction in arterioles controlling blood flow. *Am. J. Physiol.* 274:H178–H186.
13. Gustafsson, F., D. Andreasen, …, N. Holstein-Rathlou. 2001. Conducted vasoconstriction in rat mesenteric arterioles: role for dihydropyridine-insensitive Ca^{2+} channels. *Am. J. Physiol. Heart Circ. Physiol.* 280:H582–H590.
14. Seppey, D., R. Sauser, …, J. J. Meister. 2010. Intercellular calcium waves are associated with the propagation of vasomotion along arterial strips. *Am. J. Physiol. Heart Circ. Physiol.* 298:H488–H496.
15. Sneyd, J., B. T. Wetton, …, M. J. Sanderson. 1995. Intercellular calcium waves mediated by diffusion of inositol trisphosphate: a two-dimensional model. *Am. J. Physiol.* 268:C1537–C1545.
16. Höfer, T., A. Politi, and R. Heinrich. 2001. Intercellular Ca^{2+} wave propagation through gap-junctional Ca^{2+} diffusion: a theoretical study. *Biophys. J.* 80:75–87.
17. Höfer, T., L. Venance, and C. Giaume. 2002. Control and plasticity of intercellular calcium waves in astrocytes: a modeling approach. *J. Neurosci.* 22:4850–4859.
18. Hirst, G. D., and T. O. Neild. 1978. An analysis of excitatory junctional potentials recorded from arterioles. *J. Physiol.* 280:87–104.
19. Mekata, F. 1980. Electrophysiological properties of the smooth muscle cell membrane of the dog coronary artery. *J. Physiol.* 298:205–212.
20. Emerson, G. G., T. O. Neild, and S. S. Segal. 2002. Conduction of hyperpolarization along hamster feed arteries: augmentation by acetylcholine. *Am. J. Physiol. Heart Circ. Physiol.* 283:H102–H109.
21. Diep, H. K., E. J. Vigmond, …, D. G. Welsh. 2005. Defining electrical communication in skeletal muscle resistance arteries: a computational approach. *J. Physiol.* 568:267–281.
22. Koenigsberger, M., R. Sauser, …, J. J. Meister. 2004. Ca^{2+} dynamics in a population of smooth muscle cells: modeling the recruitment and synchronization. *Biophys. J.* 87:92–104.
23. Parthimos, D., D. H. Edwards, and T. M. Griffith. 1999. Minimal model of arterial chaos generated by coupled intracellular and membrane Ca^{2+} oscillators. *Am. J. Physiol.* 277:H1119–H1144.
24. Koenigsberger, M., R. Sauser, …, J. J. Meister. 2005. Role of the endothelium on arterial vasomotion. *Biophys. J.* 88:3845–3854.
25. Koenigsberger, M., R. Sauser, …, J. J. Meister. 2006. Effects of arterial wall stress on vasomotion. *Biophys. J.* 91:1663–1674.
26. Koenigsberger, M., R. Sauser, …, J. J. Meister. 2008. Calcium dynamics and vasomotion in arteries subject to isometric, isobaric, and isotonic conditions. *Biophys. J.* 95:2728–2738.
27. Parthimos, D., R. E. Haddock, …, T. M. Griffith. 2007. Dynamics of a three-variable nonlinear model of vasomotion: comparison of theory and experiment. *Biophys. J.* 93:1534–1556.
28. Moore, L. K., E. C. Beyer, and J. M. Burt. 1991. Characterization of gap junction channels in a7r5 vascular smooth muscle cells. *Am. J. Physiol. Cell Physiol.* 260:C975–C981.
29. Moore, L. K., and J. M. Burt. 1995. Gap junction function in vascular smooth muscle: influence of serotonin. *Am. J. Physiol.* 269:H1481–H1489.

30. Li, X., and J. M. Simard. 1999. Multiple connexins form gap junction channels in rat basilar artery smooth muscle cells. *Circ. Res.* 84:1277–1284.

31. Yamamoto, Y., M. F. Klemm, …, H. Suzuki. 2001. Intercellular electrical communication among smooth muscle and endothelial cells in guinea-pig mesenteric arterioles. *J. Physiol.* 535:181–195.

32. Chen, X. L., and C. M. Rembold. 1995. Phenylephrine contracts rat tail artery by one electromechanical and three pharmacomechanical mechanisms. *Am. J. Physiol.* 268:H74–H81.

33. Richards, G. R., A. H. Weston, …, G. Edwards. 2001. Suppression of K^+-induced hyperpolarization by phenylephrine in rat mesenteric artery: relevance to studies of endothelium-derived hyperpolarizing factor. *Br. J. Pharmacol.* 134:1–5.

34. Kusters, J. M., W. P. van Meerwijk, …, C. C. Gielen. 2008. Fast calcium wave propagation mediated by electrically conducted excitation and boosted by CICR. *Am. J. Physiol. Cell Physiol.* 294:C917–C930.

35. Höfer, T. 1999. Model of intercellular calcium oscillations in hepatocytes: synchronization of heterogeneous cells. *Biophys. J.* 77: 1244–1256.

36. Bezprozvanny, I., J. Watras, and B. E. Ehrlich. 1991. Bell-shaped calcium-response curves of Ins(1,4,5)P3- and calcium-gated channels from endoplasmic reticulum of cerebellum. *Nature.* 351:751–754.

37. Kaftan, E. J., B. E. Ehrlich, and J. Watras. 1997. Inositol 1,4,5-trisphosphate (InsP3) and calcium interact to increase the dynamic range of InsP3 receptor-dependent calcium signaling. *J. Gen. Physiol.* 110:529–538.